Temporal Distributions: A New Tool for the Development of Mixing Indexes for Scale-up of Polymer Processing Equipment

ARTICLE *in* POLYMER ENGINEERING AND SCIENCE · JUNE 2001

Impact Factor: 1.52 · DOI: 10.1002/pen.10807

2 AUTHORS, INCLUDING:

Ica Manas
Case Western Reserve University
135 PUBLICATIONS **1,767** CITATIONS

Temporal Distributions: The Basis for the Development of Mixing Indexes for Scale-up of Polymer Processing Equipment

WINSTON WANG *and* ICA MANAS-ZLOCZOWER*

Department of Macromolecular Science
Case Western Reserve University
Cleveland, OH 44106

New and better mixing criteria are needed to assess dispersive and distributive mixing efficiency in polymer processing equipment. Such criteria can serve the purpose of process optimization and machine scale-up. In this work, the history of flow strength and shear stresses experienced by a number of particles in a twin-flight, single-screw extruder serve as the basis to produce temporal distributions of these parameters. In turn, the temporal distributions can be used for developing new mixing indexes for process optimization and scale-up. Using models for dispersion kinetics and experimental data, calculations of agglomerate size distribution and average agglomerate size can be used as a dispersive mixing criterion.

INTRODUCTION

Mixing is an important component of most polymer processing operations. Material processability and product properties are highly influenced by mixing quality. Our research is focused on identifying the important design and processing parameters enhancing realization of the mixing process in various processing equipment and defining mixing criteria for process optimization and equipment scale-up.

Successful optimization and scale-up is a crucial part of design and operation of processing equipment. Large mixing devices often require more raw material and power in order to operate. Thus, it is impractical and inefficient to have multiple test runs to achieve optimal operating conditions, and even more so for finding optimal design parameters. The main discrepancy in scale-up stems from the fact that as machines get larger, the volume per unit length of a mixer increases with the square of the scale factor while the surface areas of equipment only increase linearly.

In the case of internal mixers, some studies (1–4) promote the concept of using the energy input as a decisive criterion for scale-up. Alternatively, the overall shear strain (1, 5) and the Weber number (6) have also been used as scale-up criteria for batch mixers. Kawanishi *et al.* preformed experimental tests on laboratory scale Banbury mixers with interchangeable rotors to duplicate rubber blending results of industrial scale mixers (7).

In the scale-up of continuous mixers, all variables of interest are expressed as a power of a characteristic ratio, such as the diameter ratio. Traditionally, scale-up strategies have been developed for single-screw extruders (8–12), and they are primarily based on constant shear rate or constant heat transfer.

Christiano (13) compared different methods of scale-up for co-rotating twin-screw extruders, based on maintaining constant thermal conduction, constant specific energy or constant residence time. White and Chen (14) performed non-isothermal flow simulations in a modular co-rotating twin screw extruder and discussed the implications of non-isothermal effects for scale-up. Nakatani proposed an "adiabatic index" criteria of keeping the resin temperature unchanged during scale-up of a twin-screw extruder (15).

In general, not all parameters can be kept the same in scale-up, and choices have to be made. If one considers scale-up designed to ensure mixing efficiency, appropriate scale-up criteria for mixing need to be defined. Selecting such criteria and applying them in complex flow geometries pose enormous challenges.

At this point, it is useful to distinguish between the different mixing mechanisms in polymer processing.

*Corresponding author.
Ica Manas-Zloczower
Department of Macromolecular Science
2100 Adelbert Rd.
Kent Hale Smith Bldg.
Case Western Reserve University
Cleveland, OH 44106

The mixing mechanism associated with the reduction in size of one component having a cohesive character, within a continuous liquid phase is referred to as dispersive mixing. The component with a cohesive character may be an agglomerated solid, a liquid droplet or a gas bubble.

In dispersive mixing, agglomerated particles or droplets held together by interfacial tension must be subjected to mechanical stress in order to reduce their length scale. Therefore, the most important flow characteristics determining dispersive mixing efficiency are the flow strength (elongational flow components) and the magnitudes of shear stresses generated.

Another mixing mechanism, occurring in the absence of a cohesive resistance, is referred to as nondispersive or extensive mixing. This type of mixing may be either distributive (rearrangement process) or laminar (achieved through deformation).

In distributive mixing, repeated rearrangement of the minor component enhances system homogeneity. In continuous mixing processes, composition uniformity at the emerging stream is directly related to the material residence time distribution. On the other hand, laminar mixing can be correlated with strain distribution functions.

Lately there has been a great deal of interest in development of mixing criteria. Many different approaches have been taken by various groups. Yao *et al.* (16) used a local mixing efficiency criteria based on the specific rate of stretching of interfacial area to analyze distributive mixing in a pin mixing section for single screw extruders. Their results are limited to a 2D finite difference analysis. Lawal and Kalyon (17) simulated the isothermal flow in single and co-rotating twin screw extruders and used various tools of dynamics to quantify distributive mixing. Kwon *et al.* proposed using "deformation characteristics" based on the Green deformation tensor as a strain and implicit mixing measure of screw extrusion processes (18).

Passive tracers have often been used to help evaluate mixing in a variety of equipment. These passive tracers are assumed to not affect the flow field and not interact with each other. Wong and Manas-Zloczower (19) studied distributive mixing in internal mixers by tracking the motion of passive tracers. Distributive mixing was quantified in terms of the probability density function of a pairwise correlation function. Avalosse used a similar technique to study mixing in a stirred tank (20). Mackley and Saraiva used kinematic mixing rates and concentration distributions of passive tracers to look at mixing in oscillatory flow within baffled tubes (21). Yoshinaga *et al.* numerically simulated distributive mixing in a twin screw extruder using residence time distributions and distribution of length stretch between tracers (22). Li and Manas-Zloczower (23, 24) and Cheng and Manas-Zloczower (25) have also used tracers to study the dynamics of the mixing process and proposed several criteria to quantify distributive mixing. Shearer and Tzonganakis used reactive polymer tracers as a microscopic probe of the interfacial surface area between two polymer melts and found a nonlinear relationship between screw speed and mixing performance (26).

Residence time distributions have been studied in conjunction with their use in evaluating the distributive mixing in processing equipment. Gao *et al.* modeled and analyzed the mean residence time and residence time distribution in a twin-screw extruder (27). They and Gasner *et al.* found a correlation between percent drag flow and residence time (27, 28). That is, a larger percentage of drag flow meant the fraction of residence time in the mixing elements decreased, resulting in poorer mixing quality.

Development of dispersive mixing criteria also poses big challenges. Gale evaluated mixing by looking at photomicrographs of samples from extruders, and discussed the limitations of using a single-screw extruder for dispersive mixing (29). Manas-Zloczower and Tadmor (30) looked at the distribution of number of passes over the flights in single screw extruders, as a way to assess dispersive mixing performance. Vainio *et al.* used the shape of the residence time distribution to evaluate dispersive mixing efficiency (31).

In this work, we focus on defining mixing indexes for scale-up in reference to the equipment dispersive mixing capability.

DISPERSIVE MIXING CHARACTERIZATION

Studies of droplet breakup in simple shear and pure elongational flows have shown that elongational flows are more effective, especially in the case of polymeric blends with high viscosity ratios and low interfacial tension (32–36). The magnitude of the applied stresses can also affect the morphology of the resulting blend. Manas-Zloczower and Feke (37, 38) posited the same conclusion for the dispersion of solid agglomerates in liquids.

As in work previously done by our group (39–41), the dispersive mixing efficiency of a flow field can be characterized in terms that account for the elongational flow contribution and the magnitude of stresses generated.

One simple way to quantify the elongational flow components is to compare the relative magnitudes of the rate of deformation, $|\underline{\underline{D}}|$, and the vorticity, $|\underline{\underline{\omega}}|$, tensors. The parameter λ_{old}, defined as:

$$\lambda_{old} = \frac{|\underline{\underline{D}}|}{|\underline{\underline{D}}| + |\underline{\underline{\omega}}|} \tag{1}$$

can be used as a basic measure of the mixing efficiency when assessing machine design and/or operating conditions. λ_{old} is equal to one for pure elongation, 0.5 for simple shear and zero for pure rotation. Therefore, the closer the value of λ_{old} to one, the better the dispersive mixing efficiency.

A more rigorous method to quantify the elongational flow components is by employing a flow strength parameter, S_f, that is frame invariant:

$$S_f = \frac{2(tr\,\underline{\underline{D}}^2)^2}{tr\,\overset{\circ}{\underline{\underline{D}}}^2} \quad (2)$$

where $\overset{\circ}{\underline{\underline{D}}}$ is the Jaumann time derivative of $\underline{\underline{D}}$ i.e. the time derivative of $\underline{\underline{D}}$ with respect to a frame of reference rotating with the same angular velocity as the fluid element. The parameter S_f ranges from zero for pure rotational flow to infinite for pure elongational flow. A simple shear flow corresponds to a S_f value of one. For consistency the flow strength parameter can be normalized according to:

$$\lambda_{new} = \frac{S_f}{1 + S_f} \quad (3)$$

Like λ_{old}, λ_{new} is equal to one for pure elongation, 0.5 for simple shear and zero for pure rotation. Calculations for λ_{new} require the second derivatives of the velocities, and is therefore more sensitive to mesh design. A higher uniform mesh density has to be used in order to reduce numerical errors.

Flow field calculations allow computation of volumetric distributions of shear stress and the parameters λ_{old} and, λ_{new}. Although useful, especially in terms of defining trends, this type of global characterization does not reflect the actual dynamics of the dispersive mixing process.

Dispersive mixing requires a process of repeated ruptures of the dispersed phase. This is accomplished by repeated passages in regions of the system where stress levels above a given threshold value are applied. The number of passages of a fluid element through high stress regions within a given residence time in the equipment depends on the particular pathline of the fluid element. Different fluid elements experience different stress histories and consequently the dispersed phase varies in size.

The discussion above suggests that in order to optimize mixing and develop valid scale-up criteria, detailed knowledge of the mechanisms of flow in the equipment is essential.

DESCRIPTION OF METHOD

In our group we carried out three-dimensional, isothermal *flow simulations* for various batch and continuous mixing equipment (23–25, 30, 40–48).

We first looked at the flow patterns in a twin-flight single-screw extruder. A fluid dynamics analysis package-FIDAP, using the finite element method was employed to solve the 3D, isothermal flow of a Newtonian fluid. No slip boundary conditions on the screw surfaces and barrel walls were used. The operating conditions were selected such that 1 clockwise revolution of the screw was made per unit time, and a pressure difference applied across the inlet and outlet surfaces satisfied the condition of $Q_p/Q_d = -1/2$. Here Q_d is the drag flow, whereas Q_p is the pressure flow in a single-screw extruder. The drag flow component Q_d was obtained in a simulation for which no pressure difference was applied. The normal stress difference was then adjusted at the inlet and outlet planes until the overall flow rate was equal to one-half that of Q_d.

FIMESH, a mesh generator that is part of FIDAP, was used to create the computer model.

The equations of continuity and motion for the steady state, isothermal flow of an incompressible Newtonian fluid were solved:

$$\underline{\nabla} \cdot \underline{V} = 0 \quad (4)$$

$$\underline{\nabla} \cdot \rho \underline{V}\,\underline{V} = \underline{\nabla}\,\underline{V} - [\underline{\nabla} \cdot \underline{\underline{\tau}}] \quad (5)$$

The Cray T-90 at the Ohio Supercomputer Center running FISOLV was used to solve the field equations. The calculations required 395 user CPU seconds over a total elapsed time of 860 seconds and 11.8 MWord of memory.

We have used an algorithm for *particle tracking* and followed the shear rate/stress histories for a number of tracers/minor component elements placed randomly at the inlet of the system. In work previously done by our group (19, 47), an algorithm was developed for tracking massless points that affect neither the flow field nor other particles. Since the flow field is completely deterministic, the location of the particles can be found by integrating the velocity vectors:

$$\underline{X}(t_1) = \underline{X}(t_0) + \int_{t_0}^{t_1} \underline{V}(t)\,dt \quad (6)$$

where $\underline{X}(t_1)$ is the location of a particle at any time t_1, $\underline{X}(t_0)$ is the location of the same particle at initial time t_0, and $\underline{V}(t)$ is the corresponding velocity vector of the particle. The location of each particle is calculated every 0.0001 time step.

We used a coordinate system that rotates with the same angular velocity as the screw, so that one finite element model can be used for all calculations. Since boundary conditions at the entrance and exit of the extruder are determined via a pressure drop, we need to minimize errors in the flow field. We do this by tracking the particles only in the center portion of the extruder. We place all the initial particles either in predetermined positions, or randomly in the extruder at an axial position Z=8. This corresponds to the beginning of the second pitch, which is the center of the model, and thereby the most accurate part of the simulation. We then track the particles until they move a distance of ±5 in the z direction, at which point the particles are repositioned one pitch back in the model and their motion resumes. In this way, we can simulate an infinitely long extruder via repeated repositioning of the particles. The particles are allowed to move from Z=3 to Z=13, which in addition to one full pitch includes a buffer zone that allows particles to change directions without a lot of extra repositioning. The number of repositions is recorded for each particle so that the actual distance traveled in the z-direction can be calculated. Because of the no-slip boundary conditions, a particle that runs into, or overshoots, a wall is considered to be stuck there and no longer moves.

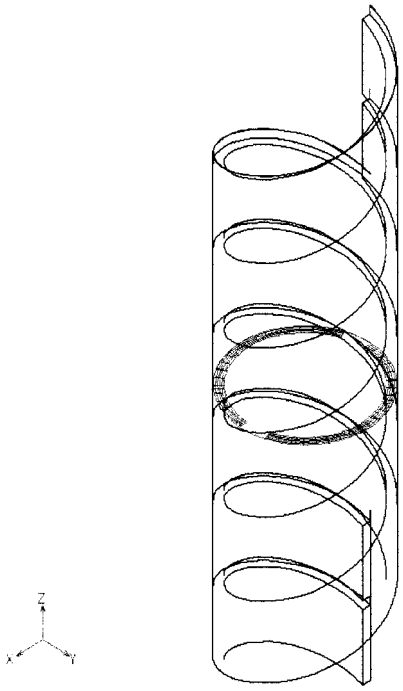

Fig. 1. 3-D schematic of the calculation domain with the mesh of the center cross section displayed.

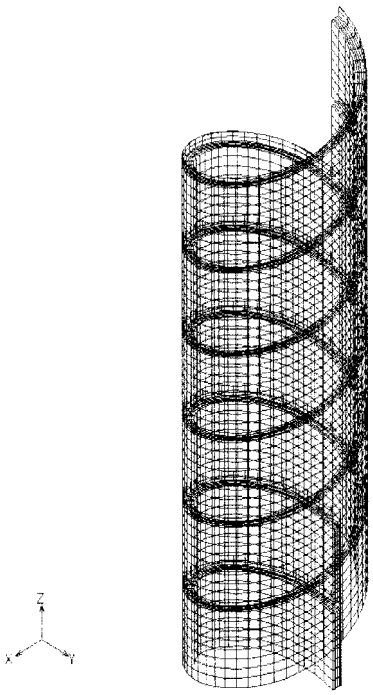

Fig. 2. Finite element mesh used.

RESULTS AND DISCUSSION

The radius of the barrel was 4.009623, and the radius of the screw was 3.534884, the flight clearance was 0.0096, and the flights were 0.44 thick (all dimensions are in arbitrary but consistent length units.)

The finite element mesh contains 16,200 8-node brick fluid elements, and 8340 4-node quadrilateral boundary elements, for a total of 20535 nodes. *Figure 1* shows a 3-D illustration of the calculation domain, including the mesh of the center cross section. *Figure 2* shows the complete finite element mesh used.

Figures 3 and *4* show the distribution plots for λ_{old} and λ_{new}, respectively, at the center cross section in the twin-flight single-screw extruder. The two plots show similar characteristics, with the majority of the fluid experiencing simple shear flow, and at the root of the flights, rotational flow. *Figure 5* displays the shear rate/stress (for a Newtonian fluid) distribution at the center cross section of the extruder. The darkest regions are where the shear rates are over 200 s^{-1}, and the lightest regions correspond to where the shear rates are under 50 s^{-1}. The flight clearance region exhibits the highest magnitude for the stresses generated.

As in our previous work, we have calculated instantaneous volumetric distributions of shear rate/stress and flow strength parameters (both frame dependent and frame invariant) (41, 45). The results are displayed in *Figs. 6–8*. The information obtained was used to assess, in a global sense, dispersive mixing efficiency. However, this type of global characterization does not reflect the actual dynamics of the mixing process.

To follow the dynamics of the mixing process, we have used several sets of particles differing only in the number of particles in the set and the method by which their initial positions are determined. All initial positions were verified to be inside the mesh design. *Figure 9* shows the initial positions for various sets of particles differing in number (for all particles the initial axial location corresponds to $Z=8$). Pathlines for

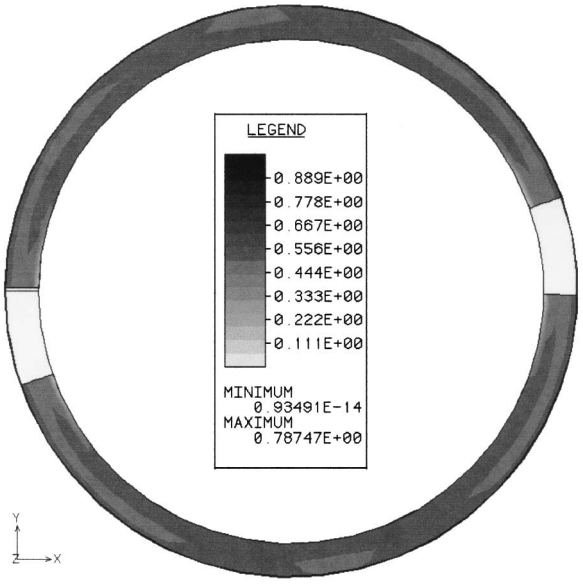

Fig. 3. Distribution plot of λ_{old} at the center cross section of the twin-flight, single-screw extruder.

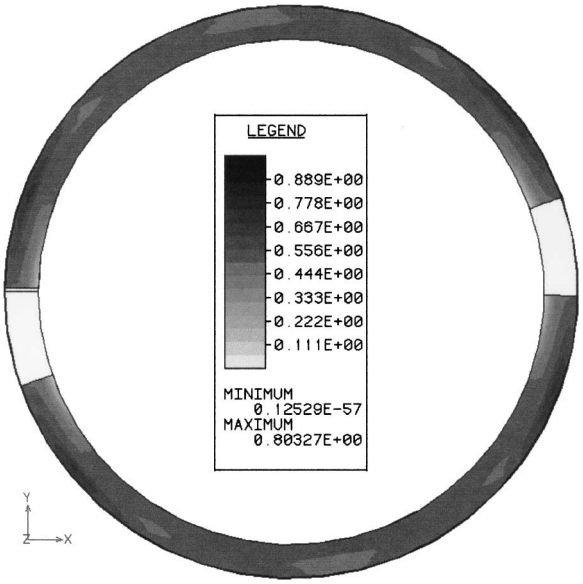

Fig. 4. Distribution plot of λ_{new} at the center cross section of the twin-flight, single-screw extruder.

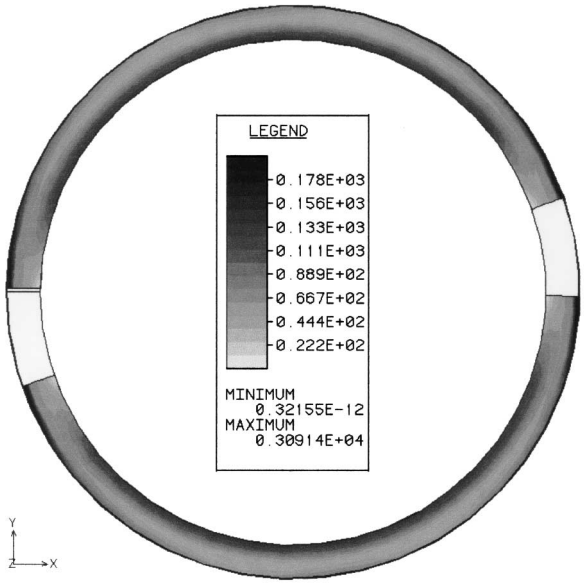

Fig. 5. Distribution plot of shear stress at the center cross section of the twin-flight single-screw extruder.

three representative particles traveling for three pitches in the extruder are shown in *Fig. 10*. The distance from the wall is the essential difference in the initial positions of particles 1, 2, and 3. Particle 3 is located closest to the barrel wall, particle 1 is located closest to the screw and particle 2 is located in the middle of the channel. For the time period tracked (30 time units), the particles move in the z direction up to 240 units, with the particles in the center of the channel travelling further than the particles near the walls. Particle 3 experiences primarily a cross channel motion, whereas particle 2 moves mainly in the z (axial) direction. Particle 1 is intermediate between the two extreme cases.

On each pathline, the exact flow history for the particle (flow strength and shear stress experienced) can be determined. *Figure 11* shows the shear rate history for 3 particles initially positioned in a radial array at the center of the channel for 10 time units (10 revolutions of the screw). While particle 3 experiences a nearly uniform shear rate of 65 s^{-1}, the true power of flow history shows itself in particle 1, which shows variations in the shear rate experienced between 60 and 110 s^{-1}, and particle 2, which varies in a lower shear rate region of 40–60 s^{-1}. *Figures 12* and *13* display the λ_{old} and λ_{new} history for the same particles. With particle 1, we can see periodic behavior related to the particle cycling through different parts of the extruder. The results indicate that the λ_{new} oscillates with larger magnitudes than λ_{old} because of the frame invariant nature of λ_{new}.

Particle flow history can also be used to calculate temporal shear rate and flow strength parameter distributions. Temporal distributions are histograms displaying the flow history of a number of particles in the system, up to a given time. *Figures 14* and *15* show the temporal distributions for the flow strength parameters (λ_{old} and λ_{new}) calculated for 500 particles up to a time of 30 units. The temporal distributions of the flow strength parameters share the same characteristics as the volumetric distributions since the flow type was relatively uniform throughout the extruder. In *Fig. 16*, the shear rate temporal distribution for the same particles is presented.

Particle tracking also allows one to calculate residence time distribution in the equipment. A histogram for the external residence time distribution for 500 particles after 30 time units in a three-pitch extruder is shown in *Fig. 17*.

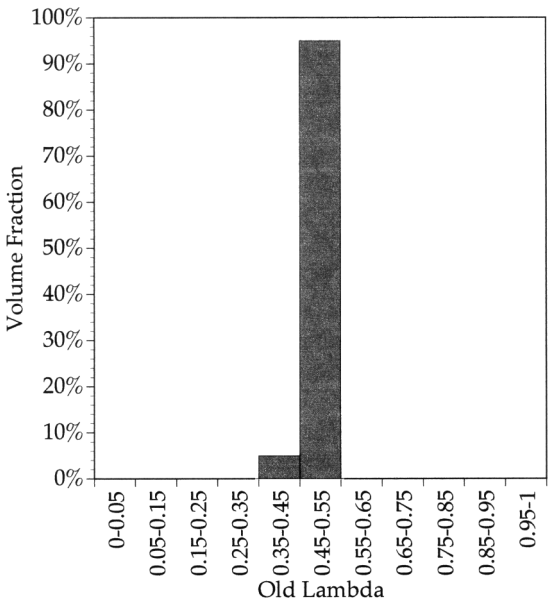

Fig. 6. Instantaneous volumetric distribution of λ_{old}.

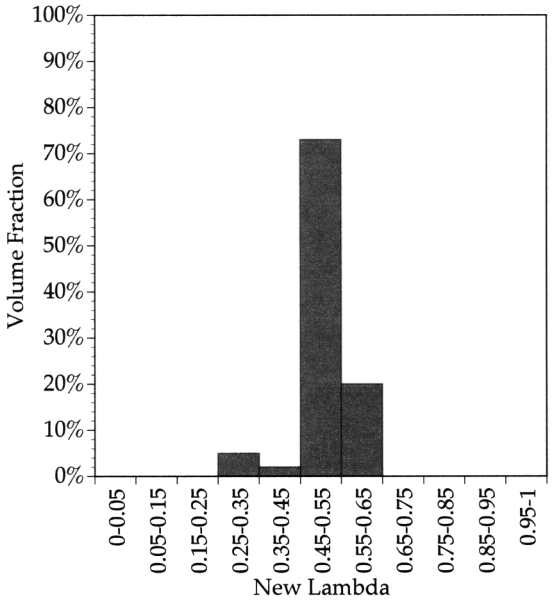

Fig. 7. Instantaneous volumetric distribution of λ_{new}.

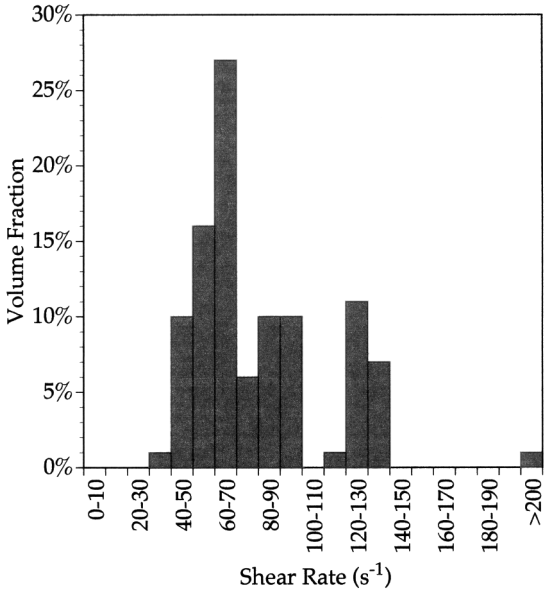

Fig. 8. Instantaneous volumetric distribution of shear rate.

PARENT AGGLOMERATE SIZE DISTRIBUTION

Recording the flow history of the particles allows one to calculate the minor component (agglomerate or droplet) size distribution at the exit from the extruder.

Previous studies of agglomerate breakup in simple shear flows (49, 50) have revealed two different dispersive mechanisms. One mechanism, denoted as erosion, is the process of gradual detachment of small fragments from the outer surface of the agglomerate. The second mechanism, rupture, is characterized by an abrupt breakage of the agglomerate into a few large pieces that can subsequently erode into smaller fragments. Since the erosion mechanism provides the fine fragments that are desirable in typical material processing, we focus on this mechanism and the kinetics of the erosion process.

Dispersion of agglomerates occurs where hydrodynamic forces acting on a fragment exceed the cohesive forces at the connection points to its parent cluster. For relatively sparse agglomerates in simple shear flows, erosion kinetics can be described by (51):

$$-\frac{dR}{dt} = K(\beta F_h - F_c), \tag{7}$$

where R is the radius of the agglomerate, t is the time, β is a proportionality factor that reflects the fraction of the overall hydrodynamic force bearing on the fragment, K is a proportionality factor related to the structure of the agglomerate, F_h is the hydrodynamic force inducing erosion and F_c is the cohesive force resisting fragmentation. The hydrodynamic and cohesive forces can be written as:

$$F_h = \frac{5}{2}\mu\dot{\gamma}\pi R^2 \tag{8}$$

$$F_c = \kappa R^m \tag{9}$$

with μ the fluid viscosity and $\dot{\gamma}$ the shear rate. Parameter κ is a scaling factor that gauges the strength of the individual bonds between interacting particles within an agglomerate and the exponent m is a measure of packing structure in the agglomerate. m varies from 0 for sparse agglomerates to 2 for dense agglomerates (51).

Integration of the rate of erosion equation for sparse agglomerates ($m = 0$) gives:

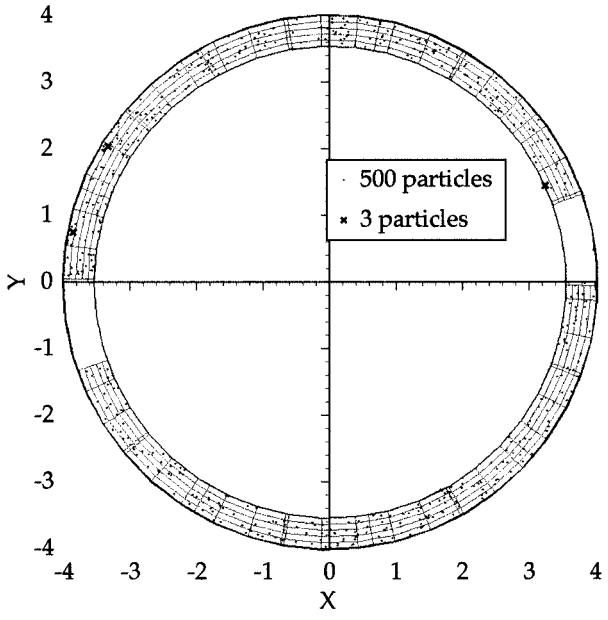

Fig. 9. XY view of initial particle positions.

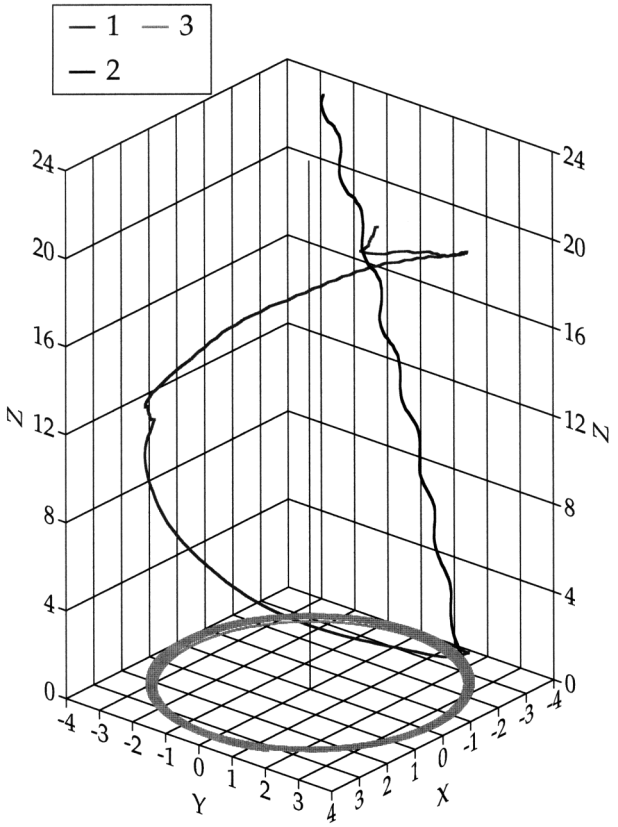

Fig. 10. Particle traces in one pitch for three particles.

$$1 - \frac{R}{R_o} = \frac{(\Theta^2 - 1)(1 - e^{-2\Theta KF_c t/R_0})}{\Theta[(1 + \Theta) + (1 - \Theta)e^{-2\Theta KF_c t/R_0}]} \quad (10)$$

where R_o is the initial agglomerate size and the parameter Θ is given by:

$$\Theta^2 = \frac{5\pi\mu\dot{\gamma}\beta R_o^2}{2F_c}. \quad (11)$$

For denser agglomerates ($m = 1$), the integration of the rate of erosion equation gives:

$$1 - \frac{R}{R_o} = 1 - \frac{be^{bt}}{b + aR_o(e^{bt} - 1)} \quad (12)$$

where,

$$a = \frac{5}{2}K\beta\mu\dot{\gamma}\pi, \quad (13)$$

$$b = Kk \quad (14)$$

As an illustrative example, previous experiments in our group studying dispersion of silica agglomerates having a density of 0.14 g/cm^3 (sparse agglomerates) in poly(dimethyl siloxane) of viscosity 60 Pa s in a cone-and-plate device (simple shear flow) yielded the following parameters for the kinetic model described by *Eq 10*: $F_c/\beta = 0.00631$ N; $KF_c = 1.102 \times 10^{-5}$ m/s (52).

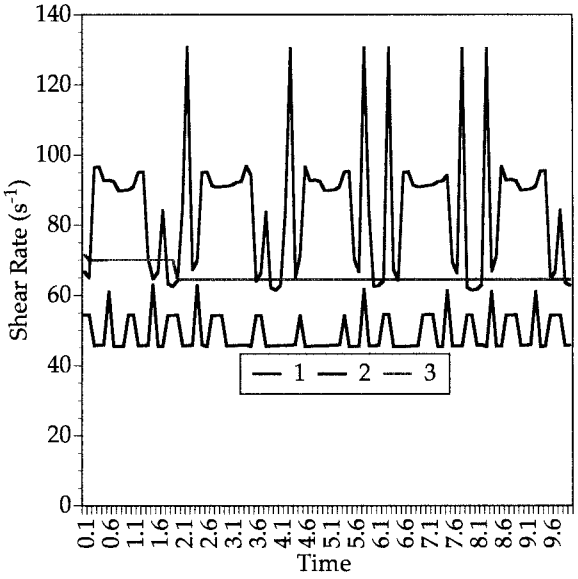

Fig. 11. Shear rate history over ten time units for three particles.

We also looked at the dispersion kinetics of carbon black agglomerates of density 0.4 g/cm^3 (medium dense agglomerates) in poly(dimethyl siloxane) of viscosity 60 Pa s in a cone-and-plate device (simple shear flow) (53) and fitted the following parameters to the kinetic model described by *Eq 12:* $K\beta = 4.0192 \times 10^{-3}$s m/kg; and $Kk = 0.055456$ s^{-1}.

As an agglomerate travels in an extruder it experiences different shear stresses as well as different flow field strengths. The kinetic models in *Eqs 10* and *12* were developed by considering erosion in simple shear flow. To account for the flow field effectiveness in

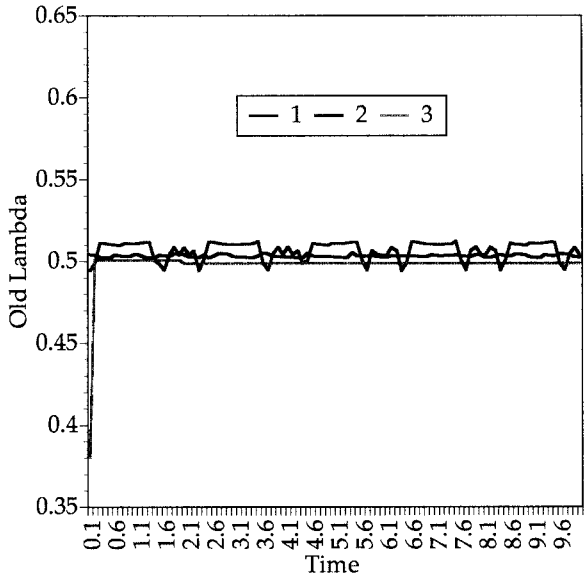

Fig. 12. λ_{old} history over ten time units for three particles.

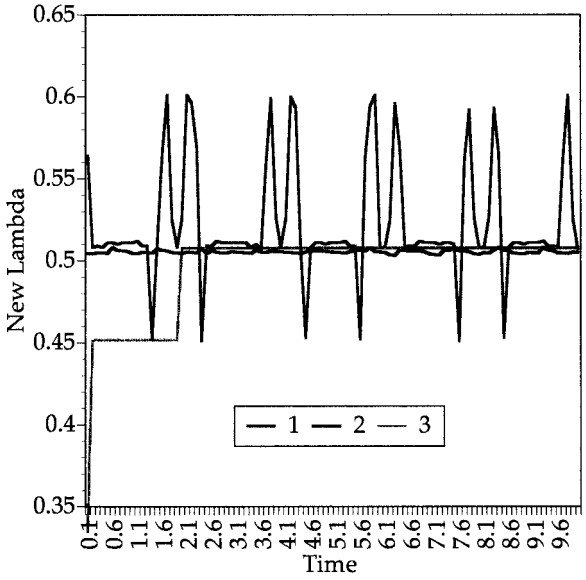

Fig. 13. λ_{new} history over ten time units for three particles.

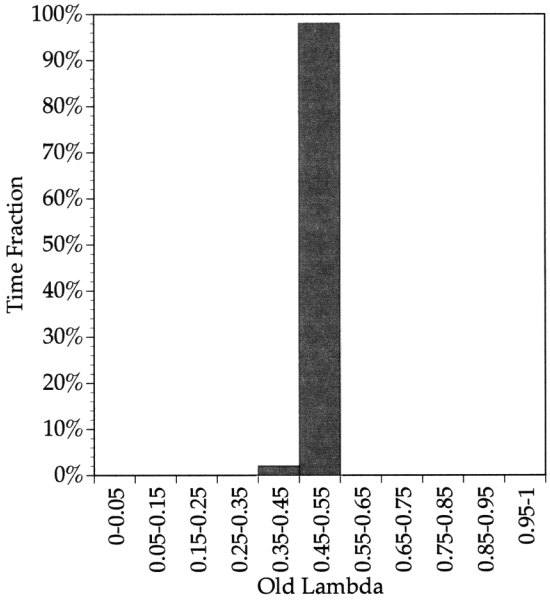

Fig. 14. Temporal distribution of λ_{old} for 500 particles for thirty time units.

agglomerate dispersion, one may consider a linear flow field as a superposition of pure extension and pure rotation. Bentley and Leal (54) and Kharkhar and Ottino (55) have shown that the critical capillary number for droplet breakup in different types of flow ranging from simple shear to pure elongation depends on the shear rate as well as on a flow strength parameter. Following their lead, we modify the expression for the hydrodynamic force on a spherical agglomerate in the principal strain direction to read:

$$F_h = 5\lambda\mu\dot{\gamma}\pi R^2 \tag{15}$$

where $\dot{\gamma}$ is the shear rate and λ is a flow strength parameter as defined in *Eq 3*. Using *Eq 15* for the hydrodynamic force will modify the parameters in the erosion kinetics model (*Eqs 10* and *12*) according to:

$$\Theta^2 = \frac{5\lambda\pi\mu\dot{\gamma}\beta R_o^2}{F_c} \tag{16}$$

and

$$a = 5\lambda k\beta\mu\dot{\gamma}\pi. \tag{17}$$

Particle flow histories were used in conjunction with the erosion kinetic models to calculate the parent agglomerate size distribution at the exit from the extruder. We have considered 500 agglomerates of initial size R_o = 1.55 mm and recorded their dispersion along a three-pitch extruder after 30 revolutions (equivalent to 30 seconds). To calculate the dynamics of particle size distribution, we account for the reduction in size of the parent agglomerate during each time step Δt by taking into consideration the actual shear rate and flow strength experienced by the particle during that time step. Also, in the kinetic models for erosion, the initial agglomerate size R_o is adjusted at each time step.

After 30 revolutions, of the 500 initial agglomerates, only 405 have exited the extruder (45 are still in the extruder and 50 hit solid surfaces and were terminated). Agglomerate size distributions for the 405 particles exiting the extruder are shown in *Fig. 18* for the case of sparse agglomerates (m = 0) and in *Fig. 19* for denser agglomerates (m = 1). As we would expect, the denser agglomerates experience less erosion. On average, the agglomerates eroded approximately 77% for m = 0 and 37% for m = 1. Also, the standard deviation of parent agglomerates (0.0828 for m = 0 and

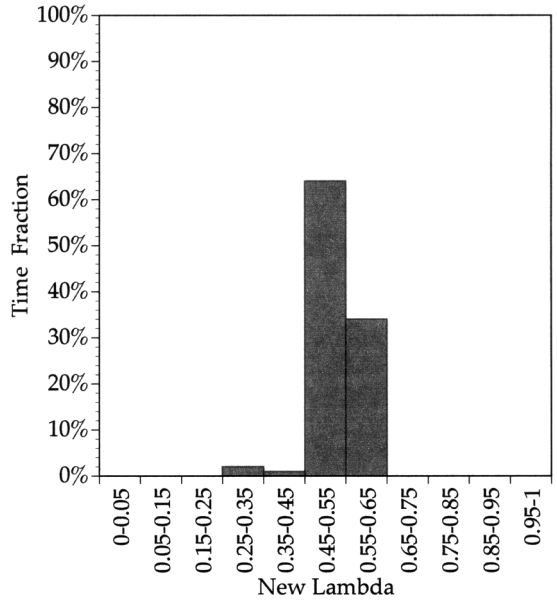

Fig. 15. Temporal distribution of λ_{new} for 500 particles for thirty time units.

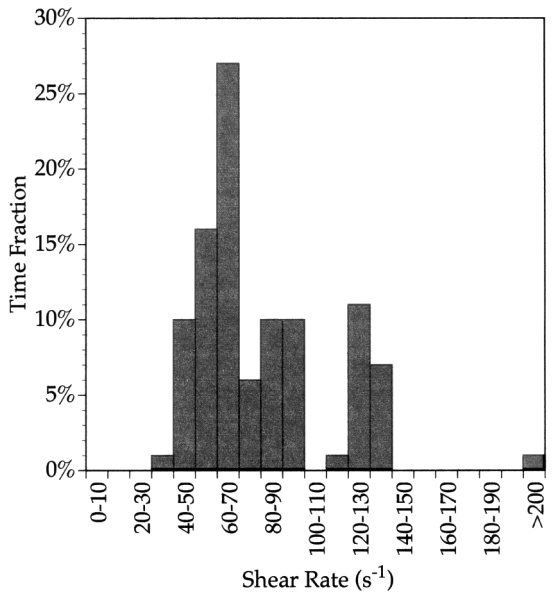

Fig. 16. Temporal distribution of shear rate for 500 particles for thirty time units.

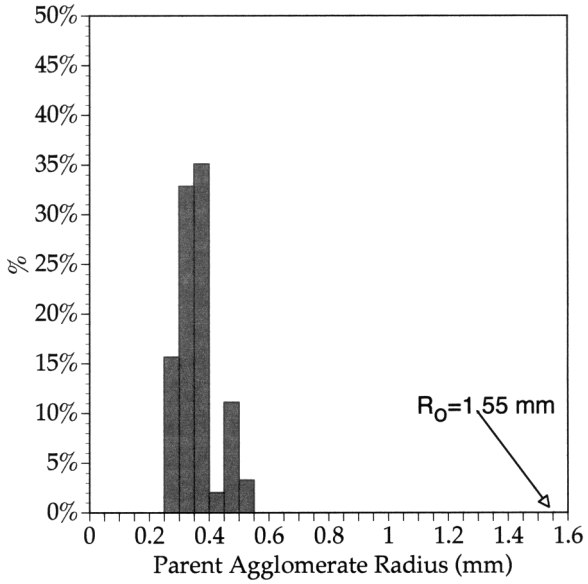

Fig. 18. Parent agglomerate size distribution for the 500 particles exiting the three-pitch extruder after thirty time units. Viscosity = 60 Pa s. Model: silica in PDMS (m=0).

0.1484 for $m = 1$) is larger for the denser agglomerates, indicating that they are more attuned to variations in the particle flow history.

CONCLUSIONS

Towards the goal of developing new mixing criteria for process control and equipment scale-up, we have presented the use of particle tracking as a method of capturing the dynamics of the mixing process. By tracking the motion of particles in the flow field we have obtained the flow history for each particle (flow strength and shear stress experienced). Using the flow history, we have calculated temporal distributions for the flow strength and shear stress in a model twin-flight single-screw extruder.

The flow history and temporal distributions form a concrete basis for developing better dispersive mixing criteria. The calculation of average agglomerate size, and agglomerate size distribution illustrate one possible avenue of developing a new dispersive mixing criterion for scale-up and optimization of mixing equipment.

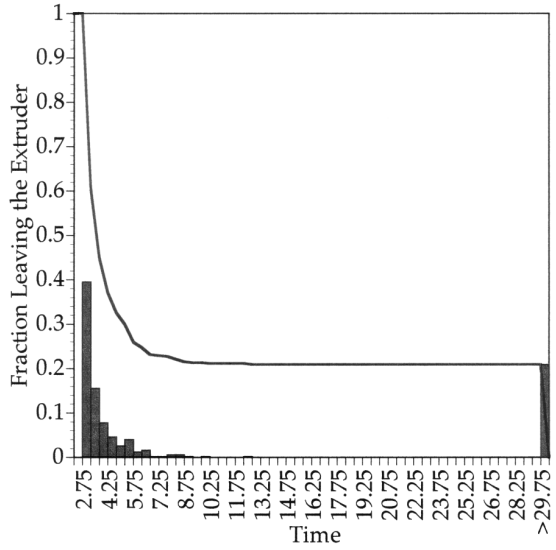

Fig. 17. External residence time distribution calculated using 500 particles for thirty time units in a three-pitch extruder. The last bin represents the fraction of particles with a residence time greater than 30 time units. The solid line illustrates the fraction of particles in the extruder at various times.

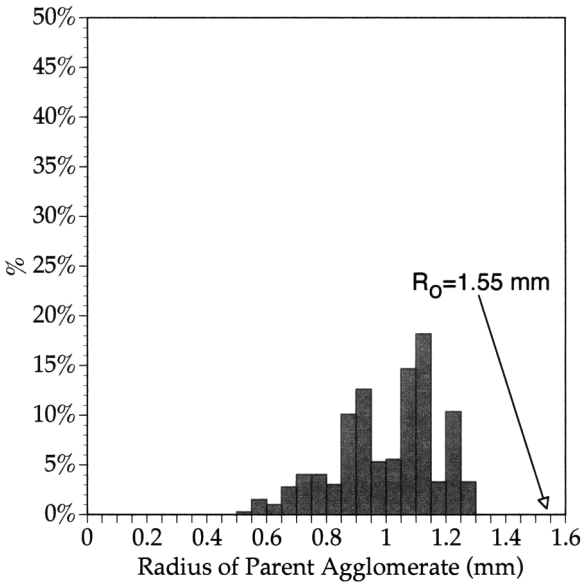

Fig. 19. Parent agglomerate size distribution for the 500 particles exiting the three-pitch extruder after thirty time units. Viscosity = 60 Pa s. Model: carbon black in PDMS (m=1).

ACKNOWLEDGMENT

The authors would like to express their gratitude to the National Science Foundation for supporting this research project under the grant DMI-9812969.

REFERENCES

1. P. R. Van Bushkirk, S. B. Turetzky, and P. F. Gunberg, *Rubber Chem. Technol.*, **48**, 577 (1995).
2. H. Palmgren, *Rubber Chem. Technol.*, **48**, 462 (1975).
3. F. S. Meyers and S. W. Newell, *Rubber Chem. Technol.*, **51**, 180 (1978).
4. J. Markert, *Kautsch. Gummi. Kunstst.*, **34**, 269 (1961).
5. J. M. Funt, *Plast. Rubber Process.*, **12**, 127 (1977).
6. J. Sunder, *Kautsch. Gummi. Kunstst.*, **43**, 589 (1990).
7. K. Kawanishi, K. Yagii, Y. Obata, and S. Kimura, *Int. Polym. Process.*, **6**, 279–289 (1991).
8. J. F. Carley and J. M. McKelvey, *Ind. Eng. Chem.*, **45**, 985 (1953).
9. J. R. A. Pearson, *Plast. Rubber Process*, **1**, 113 (1976).
10. C. I. Chung, *Polym. Eng. Sci.*, **24**, 626 (1984).
11. C. Rauwendaal, *Polym. Eng. Sci.*, **27**, 1059 (1987).
12. C. Rauwendaal, *Polymer Extrusion*, Hanser (1986).
13. J. P. Christiano, *SPE ANTEC*, **40**, 239 (1994).
14. J. L. White and Z. Y. Chen, *Polym. Eng. Sci.*, **34**, 229 (1994).
15. M. Nakatani, *Adv. Polym. Technol.*, **17**, 19–22 (1998).
16. W. G. Yao, K. Takahashi, and Y. Abe, *Int. Polym. Process.*, **11**, 222–227 (1996).
17. A. Lawal and D. M. Kalyon, *Polym. Eng. Sci.*, **35**, 1325 (1995).
18. T. H. Kwon, J. W. Joo, and S. J. Kim, *Polym. Eng. Sci.*, **34**, 174 (1994).
19. T. H. Wong and I. Manas-Zloczower, *Int. Polym. Process.*, **9**, 3–10 (1994).
20. T. Avalosse, *Macromol. Symp.*, **112**, 91–98 (1996).
21. M. R. Mackley and R. Saraiva, *Chem. Eng. Sci.*, **54**, 159–170 (1999).
22. M. Yoshinaga, *et al.*, *Polym. Eng. Sci.*, **40**, 168 (2000).
23. T. Li and I. Manas-Zloczower, *Int. Polym. Process.*, **10**, 314–320 (1995).
24. T. Li and I. Manas-Zloczower, *Chem. Eng. Commun.*, **139**, 223–231 (1995).
25. H. F. Cheng and I. Manas-Zloczower, *Polym. Eng. Sci.*, **38**, 926 (1998).
26. G. Shearer and C. Tzoganakis, *Polym. Eng. Sci.*, **39**, 1584 (1999).
27. J. Gao, G. C. Walsh, D. Bigio, R. M. Briber, and M. D. Wetzel, *Polym. Eng. Sci.*, **40**, 227 (2000).
28. G. E. Gasner, D. Bigio, C. Marks, F. Magnus, and C. Kiehl, *Polym. Eng. Sci.*, **39**, 286 (1999).
29. M. Gale, *Adv. Polym. Technol.*, **16**, 251–262 (1997).
30. I. Manas-Zloczower and Z. Tadmor, *Adv. Polym. Tech.*, **3**, 213–221 (1983).
31. T. P. Vainio, A. Harlin, and J. V. Seppala, *Polym. Eng. Sci.*, **35**, 225 (1995).
32. G. L. Taylor, *Proc. Roy. Soc.*, **A146**, 501 (1934).
33. R. L. Powelln and S. G. Mason, *AiChE J.*, **28**, 286 (1962).
34. F. D. Rumscheidt and S. G. Mason, *J. Coll. Sci.*, **16**, 238 (1961).
35. H. P. Grace, *Chem. Eng. Commun.*, **14**, 225–277 (1982).
36. J. Elmendorp, *Polym. Eng. Sci.*, **26**, 418 (1986).
37. I. Manas-Zloczower and D. L. Feke, *Int. Polym. Process.*, **4**, 3 (1989).
38. I. Manas-Zloczower and D. L. Feke, *Int. Polym. Process.*, **2**, 185 (1987).
39. C. H. Yao and I. Manas-Zloczower, *Polym. Eng. Sci.*, **36**, 305 (1996).
40. C. H. Yao and I. Manas-Zloczower, *Int. Polym. Process.*, **12**, 92–103 (1997).
41. C. H. Yao and I. Manas-Zloczower, *Polym. Eng. Sci.*, **38**, 936 (1998).
42. C. Wang and I. Manas-Zloczower, *Intern. Polym. Process IX*, **9**, 46–50 (1994).
43. C. Wang and I. Manas-Zloczower, *Intern. Polym. Process XI*, 115–120 (1996).
44. H.-H. Yang and I. Manas-Zloczower, *Int. Polym. Process IX*, 291–302 (1994).
45. H. Cheng and I. Manas-Zloczower, *Int. Polym. Process.*, **12**, 83–91 (1997).
46. H. F. Cheng and I. Manas-Zloczower, *Polym. Eng. Sci.*, **37**, 1082 (1997).
47. I. Manas-Zloczower, *Rubber Chem. Technol.*, **67**, 504–528 (1994).
48. H.-H. Yang and I. Manas-Zloczower, *Polym. Eng. Sci.*, **32**, 1411 (1992).
49. S. P. Rwei, I. Manas-Zloczower, and D. L. Feke, *Polym. Eng. Sci.*, **31**, 558 (1991).
50. S. P. Rwei, I. Manas-Zloczower, and D. L. Feke, *Polym. Eng. Sci.*, **30**, 701 (1990).
51. F. Bohin, D. L. Feke, and I. Manas-Zloczower, *Rubber Chem. Technol.*, **69**, 1–7 (1996).
52. F. Bohin, I. Manas-Zloczower, and D. L. Feke, *Chem. Eng. Sci.*, **51**, 5193–5204 (1996).
53. Q. Li, D. L. Feke, and I. Manas-Zloczower, *Rubber Chem. Technol.*, **68**, 836–841 (1995).
54. B. Bentley and L. Leal, *J. Fluid Mech.*, **167**, 241–283 (1986).
55. D. V. Khakhar and J. M. Ottino, *J. Fluid Mech.*, **166**, 265–285 (1986).